2018

Suppression of drug resistance reveals a genetic mechanism of metabolic plasticity in malaria parasites

Ann M. Guggisberg
Washington University School of Medicine in St. Louis

Philip M. Frasse
Washington University School of Medicine in St. Louis

Andrew J. Jezewski
Washington University School of Medicine in St. Louis

Natasha M. Kafai
Washington University School of Medicine in St. Louis

Aakash Y. Gandhi
Washington University School of Medicine in St. Louis

See next page for additional authors

Follow this and additional works at: https://digitalcommons.wustl.edu/open_access_pubs

Authors

Ann M. Guggisberg, Philip M. Frasse, Andrew J. Jezewski, Natasha M. Kafai, Aakash Y. Gandhi, Samuel J. Erlinger, and Audrey R. Odom John

Suppression of Drug Resistance Reveals a Genetic Mechanism of Metabolic Plasticity in Malaria Parasites

Ann M. Guggisberg,[a] Philip M. Frasse,[a] Andrew J. Jezewski,[a] Natasha M. Kafai,[b] Aakash Y. Gandhi,[a*] Samuel J. Erlinger,[a*] Audrey R. Odom John[a,c]

[a]Department of Pediatrics, Washington University School of Medicine, St. Louis, Missouri, USA
[b]Medical Scientist Training Program, Washington University School of Medicine, St. Louis, Missouri, USA
[c]Department of Molecular Microbiology, Washington University School of Medicine, St. Louis, Missouri, USA

ABSTRACT In the malaria parasite *Plasmodium falciparum*, synthesis of isoprenoids from glycolytic intermediates is essential for survival. The antimalarial fosmidomycin (FSM) inhibits isoprenoid synthesis. In *P. falciparum*, we identified a loss-of-function mutation in *HAD2* (*P. falciparum* 3D7_1226300 [PF3D7_1226300]) as necessary for FSM resistance. Enzymatic characterization revealed that HAD2, a member of the haloacid dehalogenase-like hydrolase (HAD) superfamily, is a phosphatase. Harnessing a growth defect in resistant parasites, we selected for suppression of HAD2-mediated FSM resistance and uncovered hypomorphic suppressor mutations in the locus encoding the glycolytic enzyme phosphofructokinase 9 (PFK9). Metabolic profiling demonstrated that FSM resistance is achieved via increased steady-state levels of methylerythritol phosphate (MEP) pathway and glycolytic intermediates and confirmed reduced PFK9 function in the suppressed strains. We identified HAD2 as a novel regulator of malaria parasite metabolism and drug sensitivity and uncovered PFK9 as a novel site of genetic metabolic plasticity in the parasite. Our report informs the biological functions of an evolutionarily conserved family of metabolic regulators and reveals a previously undescribed strategy by which malaria parasites adapt to cellular metabolic dysregulation.

IMPORTANCE Unique and essential aspects of parasite metabolism are excellent targets for development of new antimalarials. An improved understanding of parasite metabolism and drug resistance mechanisms is urgently needed. The antibiotic fosmidomycin targets the synthesis of essential isoprenoid compounds from glucose and is a candidate for antimalarial development. Our report identifies a novel mechanism of drug resistance and further describes a family of metabolic regulators in the parasite. Using a novel forward genetic approach, we also uncovered mutations that suppress drug resistance in the glycolytic enzyme PFK9. Thus, we identify an unexpected genetic mechanism of adaptation to metabolic insult that influences parasite fitness and tolerance of antimalarials.

KEYWORDS *Plasmodium*, antimalarial agents, drug resistance mechanisms, fosmidomycin, glycolysis, isoprenoids, malaria, metabolic regulation, metabolism

Address correspondence to Audrey R. Odom John, aodom@wustl.edu.

* Present address: Aakash Y. Gandhi, Medical Scientist Training Program, Utah, USA Southwestern Medical Center, Dallas, Texas, USA; Samuel J. Erlinger, Medical Scientist Training Program, Johns Hopkins University, Baltimore, Maryland, USA.

Malaria remains a global health threat, infecting 216 million people per year and causing nearly half a million deaths, mainly of pregnant women and young children (1). Resistance to current therapies has limited efforts to control malaria (2, 3). New drugs and a deeper understanding of drug resistance mechanisms are urgently needed.

Malaria is caused by infection with unicellular eukaryotic parasites of the genus *Plasmodium*. The species *Plasmodium falciparum* is responsible for most life-threatening malarial disease. As an obligate intracellular parasite of human erythrocytes, *Plasmo-*

dium falciparum has unique metabolic features that may be exploited to discover new drug targets and develop new therapies. In the red blood cell niche, *Plasmodium* parasites are highly dependent on glucose metabolism. Infection with *Plasmodium* spp. results in a nearly 100-fold increase in glucose import in red blood cells (4–6). Despite these energy requirements, the parasite demonstrates little aerobic respiration via the tricarboxylic acid (TCA) cycle. Instead, it relies on anaerobic glycolysis to produce ATP (7–10).

Besides ATP production, glucose also has a number of anabolic fates in *P. falciparum*. One such fate is the synthesis of isoprenoids. Isoprenoids are a large class of hydrocarbons with extensive structural and functional diversity (11). In the malaria parasite, isoprenoids perform several important functions, including protein prenylation, dolichylation, and synthesis of GPI anchors (12–14). Despite this diversity, all isoprenoids are synthesized from a common five-carbon building block, isopentyl pyrophosphate (IPP). Evolution has produced two distinct routes for IPP synthesis: the mevalonate pathway, found in archaea, fungi, animals, and the cytoplasm of plants; and the methylerythritol phosphate (MEP) pathway, found in most eubacteria, plant chloroplasts, and apicomplexan parasites such as *P. falciparum* (15). Because it is both essential for the parasite and absent from the human host, the MEP pathway is a compelling target for antimalarial development. The antibiotic and antimalarial fosmidomycin (FSM) is a competitive inhibitor of the first committed enzymatic step of the MEP pathway, catalyzed by 1-deoxy-D-xylulose-5-phosphate reductoisomerase (DXR; EC 1.1.1.267) (16–18). FSM has been validated as a specific inhibitor of the MEP pathway in *P. falciparum* (19) and is a valuable chemical tool to study MEP pathway biology and essential metabolism in the parasite. In this study, we found that FSM is also a useful tool for probing glycolytic metabolism upstream of the essential MEP pathway.

Parasites are likely to control the proportion of glucose used for energy production versus production of secondary metabolites, such as isoprenoids. We previously used a screen for FSM resistance to identify HAD1, a metabolic regulator whose loss results in increased levels of MEP pathway intermediates and resistance to MEP pathway inhibition. HAD1 is a cytoplasmic sugar phosphatase that dephosphorylates a number of sugar phosphate intermediates upstream of the MEP pathway (20, 21). HAD1 belongs to the haloacid dehalogenase-like hydrolase (HAD) enzyme superfamily and, more specifically, to the IIB and Cof-like hydrolase subfamilies (22). While HADs are found in all kingdoms of life, HAD1 is most closely related to bacterial members of this superfamily (20, 23), which have been implicated in metabolic regulation, stress response, and phosphate homeostasis (24–28). However, most members of this superfamily remain uncharacterized.

In this report, we describe the discovery of HAD2, a second HAD family member in *P. falciparum*. We found that HAD2 is a cytosolic phosphatase required for metabolic homeostasis. Loss of HAD2 dysregulates glycolysis and misroutes metabolites toward the MEP pathway, conferring drug resistance. In our study, we harnessed a fitness defect in *had2* parasite strains to employ an innovative screen for suppression of drug resistance in the parasite. Selection for suppression of drug resistance identified mutations in *PFK9*, which encodes the canonical glycolytic regulatory enzyme phosphofructokinase (PFK). Reduction in PFK9 activity rescued the metabolic dysregulation in our resistant mutants and restored FSM sensitivity. Our unique approach thus reveals PFK9 as a site of exceptional metabolic plasticity in the parasite and uncovers a novel genetic mechanism by which *P. falciparum* malaria parasites may adapt to metabolic stress and drug selective pressure.

(This article was submitted to an online preprint archive [29]).

RESULTS

An FSM-resistant (FSM^r) strain possesses a nonsense allele of *HAD2*, homolog of the MEP pathway regulator HAD1. The MEP pathway is responsible for the synthesis of the essential isoprenoid precursors isopentenyl pyrophosphate (IPP) and dimethylallyl pyrophosphate (DMAPP). This pathway is specifically inhibited by the
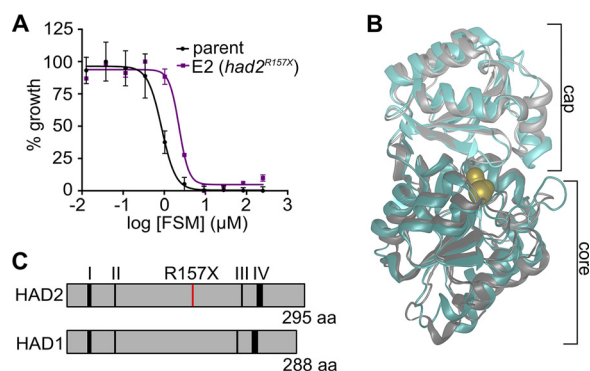
FIG 1 FSMr strain E2 possesses a mutation in HAD2, a homolog of MEP pathway regulator HAD1. (A) Representative FSM dose response of the parental strain and strain E2. (B) *P. vivax* HAD2 (teal; PDB 2B30) is structurally similar to PfHAD1 (gray; PDB 4QJB). Ions (Mg^{2+}, Ca^{2+}, Cl^-) are shown in yellow. (C) HAD2 is a homolog of HAD1 (29% identity and 53% similarity) and possesses all conserved HAD sequence motifs required for catalysis (37).

antibiotic FSM (19, 30, 31). We previously generated *P. falciparum* strains resistant to FSM. Mutations in *HAD1* (*P. falciparum* 3D7_1033400 [PF3D7_1033400]) cause the resistance phenotype in a majority of these strains (20). However, the genetic and biochemical basis of FSM resistance in strain E2 remained unknown. As previously reported, we found that E2 is less sensitive to FSM than its wild-type (WT) 3D7 parental line (Fig. 1A) (20). Strain E2 showed an FSM half-maximal inhibitory concentration (IC_{50}) of 4.8 ± 1.2 μM, significantly greater than that shown by its parent strain (0.9 ± 0.06 μM) ($P \leq 0.01$ [unpaired Student's *t* test]).

We found that this resistance phenotype was not due to changes in expression of the genes encoding the first two (rate-limiting) steps of the MEP pathway, *DXS* and *DXR* (32–35) (see Fig. S1A in the supplemental material). In addition, strain E2 does not have genetic changes in the known FSM resistance locus and MEP pathway regulator, *HAD1*, and HAD1 appears to be expressed in strain E2 (Fig. S1B).

To identify new genetic changes that may result in FSM resistance, we performed whole-genome sequencing on strain E2 and identified an A469T mutation in PF3D7_1226300 (PlasmoDB identifier [ID]), here referred to as *HAD2* (36). Variant data for strains sequenced in this study can be found in Data Set S1 in the supplemental material. Sanger sequencing of the *HAD2* locus in strain E2 confirmed the presence of the A469T single nucleotide polymorphism (SNP). The A469T SNP yielded a truncated (R157X) protein variant, and we therefore expected that HAD2 function would be lost in strain E2. Interestingly, HAD2 is a close homolog of a known MEP pathway regulator, the sugar phosphatase HAD1 (20). Sequence homology places both proteins in the haloacid dehalogenase-like hydrolase (HAD) superfamily and, further, within the IIB and Cof-like hydrolase subfamilies (Interpro IPR006379 and IPR000150, respectively) (22). While no structural information exists for *P. falciparum* HAD2, the structure of the *Plasmodium vivax* HAD2 (PVX_123945; *P. vivax* HAD2 [PvHAD2]) has been solved (PDB ID 2B30). PvHAD2 (93% identical and 98% similar to *P. falciparum* HAD2 [PfHAD2]) contains the common structural motifs found in other HADs, including a core and cap domain (Fig. 1B). HAD2 possesses the four conserved sequence motifs found in HAD proteins (Fig. 1C), which are involved in binding of the substrate, coordination of the phosphoryl group and Mg^{2+} ion, and hydrolysis of the substrate phosphate (37–39). Overall, HAD2 and HAD1 protein sequences share ~29% sequence identity and ~53% sequence similarity (Fig. 1C). We hypothesized that HAD2, like HAD1, regulates metabolism in *P. falciparum* and that loss of HAD2-mediated metabolic control was responsible for FSM resistance in malaria parasite strain E2.

HAD2 is a functional phosphometabolite phosphatase. We have previously established that *P. falciparum* HAD1 is a promiscuous sugar phosphatase, with activity against a wide range of phosphometabolites. Similarly, *P. vivax* HAD2 has been enzy-
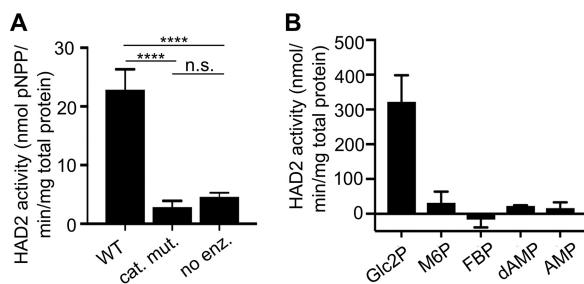
FIG 2 PfHAD2 is a phosphatase. (A) HAD2 is an active phosphatase, and HAD2[D26A] is a catalytic mutant (cat. mut.) that can be used as a negative control for HAD2-specific activity. "No enz." represents a no-enzyme control. Data shown represent the enzyme activities seen using the synthetic phosphatase substrate pNPP. Error bars represent standard errors of the means (SEM) (****, $P \leq 0.0001$ [unpaired t test]; n.s., not significant). (B) Activity of HAD2, normalized to the activity of the catalytic mutant (HAD2[D26A]), for a variety of substrates (2-GlcP, 2-glycerol-phosphate; M6P, mannose-6-phosphate; FBP, fructose-2,6-bisphosphate; dAMP, deoxy-AMP). Error bars represent SEM.

matically characterized and found to possess phosphatase activity against various monophosphorylated substrates, including glycerol 2-phosphate (glc2P) and pyridoxal phosphate (PLP) (40). Recombinant PvHAD2 also utilizes additional monophosphorylated substrates, such as AMP and glycerol 1-phosphate (glc1P), with moderate activity.

On the basis of the previous characterization of a close *Plasmodium* homolog, as well as sequence homology to HAD1 and other HAD proteins, we predicted that PfHAD2 would also function enzymatically as a phosphatase. We successfully purified recombinant PfHAD2 in *Escherichia coli* and confirmed the phosphatase activity of recombinant PfHAD2 using *para*-nitrophenyl phosphate (pNPP), a promiscuous, chromogenic phosphosubstrate (Fig. 2A) (23, 41). Because *E. coli* expresses a number of HAD-like phosphatases (23), we confirmed that the phosphatase activity was specific to purified PfHAD2 by expression and purification of a catalytically inactive mutant (HAD2[D26A]). The Asp26 residue was chosen for mutagenesis because the corresponding residue in PfHAD1 (Asp27) has been previously shown to be required for catalysis (21).

We also established the activity of PfHAD2 against a panel of phosphorylated substrates and determined that its substrate profile closely mirrors that of PvHAD2 (Fig. 2B). Overall, we found that PfHAD2 is a phosphatase with activity against small phosphosubstrates, such as glc2P. These data suggest that, like HAD1 and related HADs in microbes and plants (23, 42–44), HAD2 is a phosphatase with the potential to utilize a variety of monophosphorylated phosphometabolites.

***In vitro* evolution of mutations suppressing FSM resistance.** During routine culturing of E2 FSM[r] parasites, we observed that the E2 strain appeared to be growth attenuated compared to its parental parasite strain. Surprisingly, during prolonged culture in the absence of FSM, this growth phenotype resolved, and improved growth rates correlated with a return to FSM sensitivity (Fig. 3A). From these observations, we hypothesized that *had2[R157X]*-mediated FSM resistance led to a fitness cost in cultured parasites. We sought to harness this fitness cost to drive *in vitro* evolution of an FSM-sensitive (FSM[s]) population possessing additional, novel mutations that might suppress FSM resistance in *had2[R157X]* parasite strains.

FSM-resistant strain E2 was cultured through multiple passages in the absence of FSM selection. Through limiting dilution, we derived five E2-based clones in the absence of drug pressure (Fig. 3B). Of the five clones, three (designated clones E2-R1, E2-R2, and E2-R3) remained FSM[r], but two of these (designated E2-S1 and E2-S2) were found to be FSM[s] (Fig. 3B and 4A). To validate our novel suppressor screen approach, we independently repeated this genetic selection with the three FSM[r] E2 clones by again culturing in the absence of FSM for >1 month (Fig. 3B). As before, these strains (E2-S3, E2-S4, and E2-S5) also lost their FSM resistance phenotype (Fig. 4A).

Consistent with our initial observation that our *had2[R157X]* FSM-resistant strain grew poorly, we found that the FSM[r] clones (E2-RX) grew at a significantly reduced rate
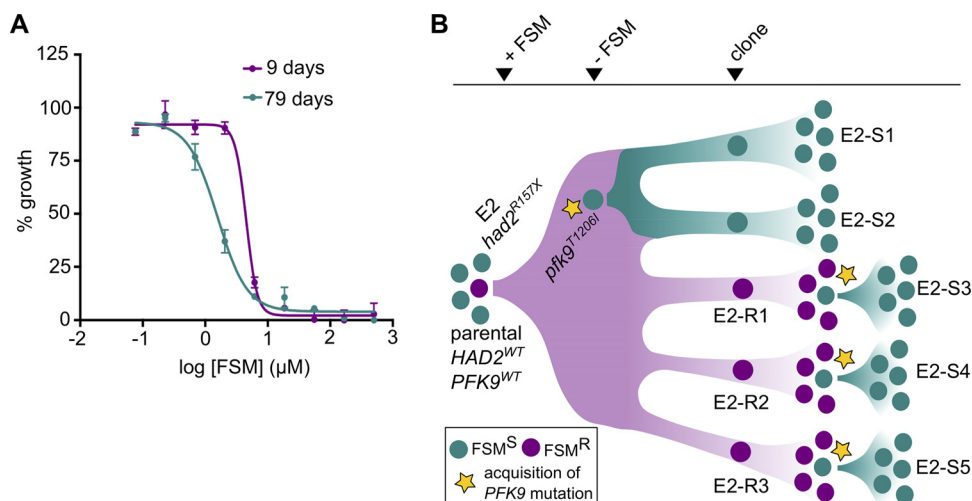
FIG 3 Leveraging resistance-associated growth attenuation to identify genetic changes that modulate FSM sensitivity. (A) Prolonged culture resulted in loss of FSM resistance in strain E2. Shown are FSM dose responses of the strain E2 before (day 9) and after (day 79) prolonged culture without FSM. Nine days after thawing resistant strain E2, we observed an FSM IC_{50} of 4.9 μM, while after 79 days of culture without FSM, E2 had an FSM IC_{50} of 1.3 μM. The dose responses were part of routine evaluation of individual strain phenotypes at discrete points in time. Each data point is representative of the mean from two technical replicates. Error bars represent SEM. (B) Parasites are colored according to FSM phenotype (teal, FSM^s; purple, FSM^r). Cloned strains are named according to FSM phenotype (E2-SX, sensitive; E2-RX, resistant). An FSM^s parental strain was selected under conditions of FSM pressure to enrich for FSM^r strain E2 ($had2^{R157X}$). After relief of FSM pressure, a fitness advantage selected for spontaneous suppressor mutations in *PFK9* ($pfk9^{mut}$; yellow star) that resulted in FSM sensitivity. FSM^r clones were grown without FSM pressure, and a fitness advantage again selected for suppressor mutations in *PFK9* that resulted in an increased growth rate and loss of FSM resistance.

compared to the parental strain, while the FSM^s clones (E2-SX) had restored growth rates similar to that of the wild-type parental strain (Fig. 4B).

Loss of FSM resistance might have occurred by reversion of the $had2^{R157X}$ mutation in E2-derived strains. Instead, we found that all E2-SX clones maintained loss of HAD2 via the $had2^{R157X}$ mutation. We hypothesized that the FSM^s E2 clones, driven by a fitness advantage, had acquired a new suppressor mutation(s) at an additional locus. We performed whole-genome sequencing on the original five E2 clones to identify any genetic changes that segregated with FSM sensitivity. Sequencing revealed that
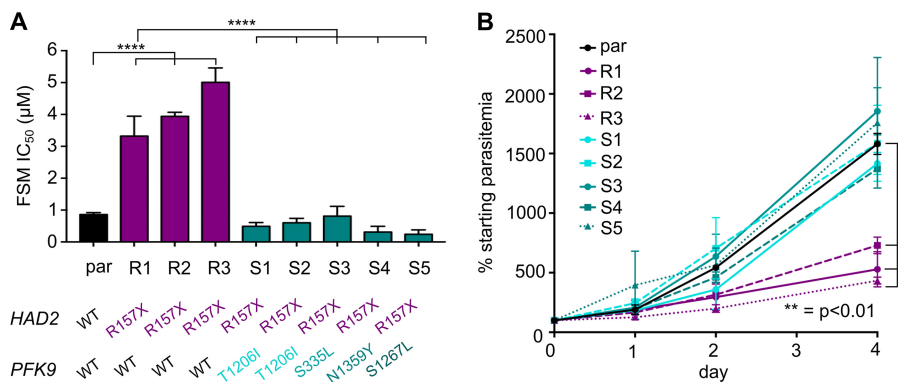
FIG 4 Suppressor strains with *PFK9* mutations display changes in FSM tolerance and growth. (A) Suppressed clones have significantly lower FSM IC_{50}s (****, $P \leq 0.0001$). Error bars represent SEM. *HAD2* and *PFK9* genotypes for each strain are indicated. For reference, the parental (par) strain data are shown in the black column. All data are representative of results from $\geq$3 independent experiments. (B) FSM resistance results in a fitness cost. FSM^r clones with the $had2^{R157X}$ allele (R1 to R3, purple lines) had reduced growth rates compared to the wild-type parental (par) strain (black) (*, $P \leq 0.05$). The growth defect was rescued in clones with mutations in *PFK9* (S1 to S5, teal lines). Growth was normalized to parasitemia on day 0. Error bars represent SEM of results from $\geq$3 independent growth experiments.

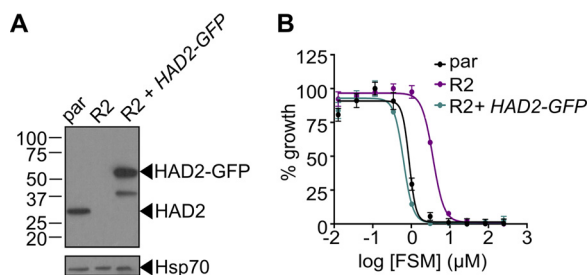**FIG 5** Loss of HAD2 is necessary for FSM resistance. (A) Successful expression of pTEOE110:HAD2-GFP in strain R2 (*had2^R157X^*, *PFK9*) was confirmed by immunoblotting. Marker units are indicated in kilodaltons (kDa). The top blot was probed with anti-HAD2 antiserum (expected masses: HAD, 33 kDa; HAD2-GFP, 60 kDa). The bottom blot was probed with anti-heat shock protein 70 (Hsp70) antiserum as a loading control. (B) Representative FSM dose response demonstrating that expression of HAD2-GFP in strain R2 (*had2^R157X^ PFK9*) resulted in restored sensitivity to FSM. Strain R2 had an elevated FSM IC$_{50}$ compared to the parental (par) strain. When HAD2 expression was restored in strain R2, the resulting strain showed an IC$_{50}$ near that of the parent strain. Data shown are from a representative clone (clone 1) of the HAD2-rescued strain. Additional clones displayed a similar phenotype (see Fig. S2).

a new mutation (C3617T) in the locus encoding phosphofructokinase-9 (*PFK9*; PF3D7_0915400) was present in both of the suppressed (FSM^s^) E2 clones but in none of the three FSM^r^ E2 clones (Fig. 3B; see also Data Set S1). The C3617T mutation results in a PFK9^T1206I^ protein variant. *PFK9* contained the only SNP that segregated with the change in FSM tolerance. Two other loci had indels that also segregated with our FSM phenotype. These loci encode a tyrosine recombinase (MAL13P1.42) (45) and an erythrocyte surface protein (PIESP1; PFC0435w). Given their predicted functions and the presence of A/T indels in poly(A) and poly(T) tracts, we concluded that mutations in these loci were unlikely to result in our suppressed phenotype and prioritized *PFK9* as the likely locus of our suppressor mutation.

To verify whether mutations in *PFK9* were responsible for suppressing FSM resistance in all of our suppressed strains, we investigated *HAD2* and *PFK9* in the E2-S3, -S4, and -S5 strains, which were derived through independent evolution of the E2-R1, -R2, and -R3 populations in the absence of FSM. By Sanger sequencing, we found that, as before, all strains maintained the *had2^R157X^* mutation and acquired new, independent *PFK9* mutations (Fig. 4A). The independent acquisition of four different *PFK9* alleles during selection, each of which was associated with both improved growth and loss of FSM resistance, strongly indicates that loss of PFK9 function is responsible for these phenotypes in strains lacking HAD2.

Loss of HAD2 is necessary for FSM resistance in *had2^R157X^* parasites. HAD2 was not the sole genetic change in FSM^r^ strain E2. In addition, because intraerythrocytic *P. falciparum* parasites are haploid, we cannot distinguish recessive from dominant or gain-of-function mutations. Therefore, we sought to establish whether restoring HAD2 expression in *trans* in a *had2^R157X^* strain would restore FSM sensitivity. Using a previously described expression system enabled by the piggyBac transposase (20, 46), we expressed HAD2-green fluorescent protein (HAD2-GFP) driven by the heat shock protein 110 (Hsp110) promoter (47). We confirmed that the transfected *had2^R157X^* E2-R2 clone maintained the *had2^R157X^* allele at the endogenous locus and successfully expressed HAD2-GFP (Fig. 5A). Additionally, the *had2^R157X^* allele does not appear to result in a truncated protein product, as evidenced by immunoblotting of the E2-R2 clone and the corresponding rescued strain (Fig. 5A). This suggests that complete loss of HAD2, as opposed to a truncated protein isoform, is responsible for the observed phenotypes in the E2-RX mutants. Expression of HAD2-GFP in *had2^R157X^* parasites results in restoration of FSM sensitivity (Fig. 5B; see also Fig. S2), confirming that loss of HAD2 is necessary for FSM resistance in this strain. The resistant clone (E2-R2) has an FSM IC$_{50}$ of 3.9 ± 0.2 μM, significantly higher than that of the wild-type parent strain (0.9 ± 0.06 μM, *P* ≤ 0.001 [one-way analysis of variance {ANOVA} and Sidak's posttest]). Expression of HAD2-GFP in E2-R2 results in an IC$_{50}$ of 0.6 ± 0.02 μM for FSM, signifi-
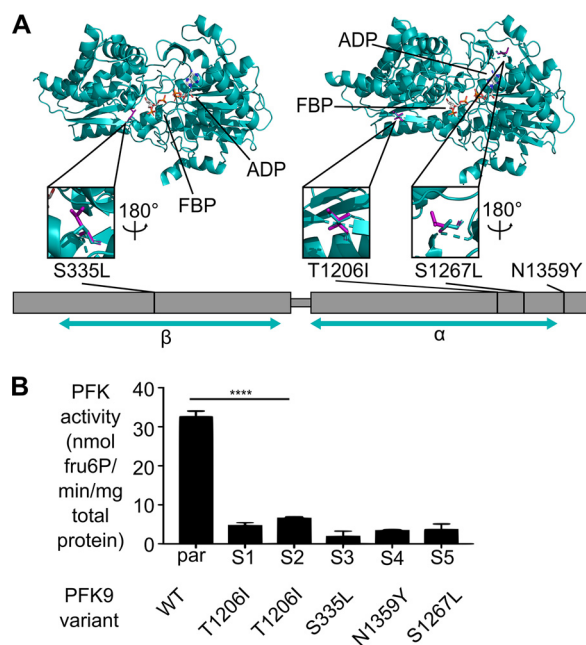
FIG 6 *PFK9* alleles in suppressed strains are hypomorphic. (A) Schematic of suppressor mutations found in *PFK9*. Strain names and resulting amino acid changes are indicated. Three of the four mutations are found on the structural model of PfPFK. The parts of the protein represented by the model are notated by the teal arrows under the α and β domains. The total protein length is 1,418 amino acids. N1359Y fits outside the model. The other mutations are represented by their stick model structure, with the resulting change shown in magenta. Orientations of the closeup representations of the mutations are indicated where they differ from the main model. (B) Measurement of PFK activity of *P. falciparum* lysate indicated that E2-SX clones with *PFK9* suppressor mutations have significantly reduced PFK activity (****, $P \leq 0.0001$ [ANOVA, Sidak's posttest]). Error bars represent SEM. Assay data are linear with respect to protein content and specific for PfPFK9 activity (Fig. S3).

cantly lower than that seen with the E2-R2 strain ($P \leq 0.001$) but not significantly different from that of the parental strain ($P > 0.5$).

Using fluorescence microscopy, we also investigated the localization of HAD2-GFP in our E2-R2 Hsp110:HAD2-GFP strain. We observed that HAD2-GFP was diffusely present throughout the cytoplasm in asexual *P. falciparum* trophozoites and schizonts but excluded from the digestive food vacuole (Fig. S3). This finding is consistent with the lack of a predicted signal sequence for HAD2 as determined using SignalP, PlasmoAP, and PlasMit algorithms (48–50).

PFK9 mutations in suppressed strains are hypomorphic. The *PFK9* locus encodes the enzyme phosphofructokinase (PFK; EC 2.7.11), which catalyzes the first committed and canonically rate-limiting step of glycolysis, which is the conversion of fructose 6-phosphate to fructose 1,6-bisphosphate. PFK9 is comprised of two domains, alpha (α) and beta (β), which are typically encoded by independent genes in nonapicomplexans (51) (Fig. 6A). While in other systems the α domain is regulatory, previous work on *P. falciparum* PFK9 has demonstrated catalytic activity for both domains (51–55).

Of the four PFK9 variants identified in this study, three variants map to the α domain, while one variant (S335L) maps to the β domain (Fig. 6A). We projected our mutations onto a three-dimensional model of PfPFK9 to reveal a possible structural basis for altered PFK function. Three variants (S335, T1206I, and S1267L) align to and model currently available crystal structures of PFK, while a fourth allele (N1359Y) does not. While three (T1206I, S1267L, and N1359Y) of the four mutations map to the α domain of PfPFK9, these mutations do not appear to cluster in any particular region. All mutations affect amino acid residues that are physically distant from the substrate-binding pocket of either domain and are not predicted to impact binding or specific catalytic residues.
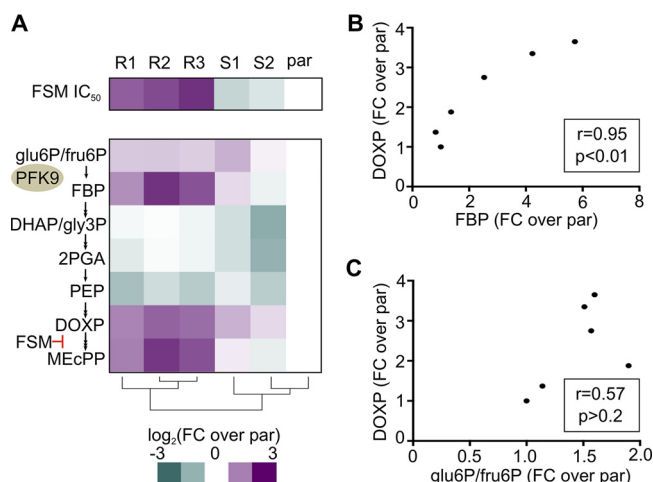
FIG 7 *HAD2* and *PFK9* alleles alter FSM resistance and metabolite levels in *P. falciparum*. (A) Metabolic profiling and clustering of parental (par) and E2 clone strains demonstrated a metabolic signature of resistance, which included increased levels of MEP pathway intermediates DOXP and MEcPP and the glycolytic metabolite and PFK product FBP. Glu6P/fru6P and DHAP/gly3P are isomer pairs that cannot be confidently distinguished. Clustering was performed using the heatmap function in R. Data are also summarized in Table S1 and Fig. S5. FSM IC$_{50}$s are shown for reference. FC, fold change. (B) DOXP levels were highly correlated to levels of the upstream glycolytic metabolic FBP (Pearson's $r = 0.95$). (C) By contrast, DOXP levels were not correlated to the glycolytic metabolites glu6P/fru6P (Pearson's $r = 0.57$).

Consistent with a previous study on PfPFK9 (51), attempts to purify recombinant full-length PFK9 were unsuccessful. Thus, to understand the enzymatic impacts of our PFK9 variants, we quantified the native PFK-specific activity in *P. falciparum* (51, 56) (Fig. 6B; see also Fig. S4). Lysates from strains possessing *PFK9* mutations (E2-SX strains) have markedly reduced specific activity of PFK compared to the parental strain (Fig. 6B). Combined with the diverse mutation locations (Fig. 6A), the reduced lysate PFK activity in E2-SX strains suggests that a variety of genetic strategies to alter PFK function can lead to resistance suppression.

Metabolic profiling reveals mechanisms of resistance and suppression in *HAD2* and *PFK9* mutant parasites. Reduced activity of PFK9, which catalyzes the canonical rate-limiting step in glycolysis, is associated with restored FSM sensitivity of *had2* mutant strains. Therefore, we anticipated that metabolic changes might underlie both resistance and suppression in our E2 clones. We performed targeted metabolic profiling on the parental parasite strain as well as E2 clones R1 to R3 and S1 and S2 (Fig. 7A; see also Table S1 and Fig. S5 in the supplemental material). We found that levels of the MEP pathway intermediate DOXP (1-deoxy-D-xylulose 5-phosphate) were significantly increased in FSM^r (*had2*^{R157X} *PFK9*) strains (Fig. 7A) ($P \leq 0.05$ [one-way ANOVA and Sidak's posttest]). FSM is competitive with DOXP for inhibition of its target enzyme, DXR. Therefore, our data are consistent with the hypothesis that FSM^r strains achieve resistance via increased levels of DOXP, which outcompetes FSM. We also observed a significant increase in the downstream MEP metabolite, MEcPP (2-C-methyl-D-erythritol-2,4-cyclopyrophosphate), in our FSM^r strains ($P \leq 0.05$).

To understand the role of PFK9 in conferring and suppressing FSM resistance, we determined the steady-state levels of intermediates from glycolysis, metabolites of which feed into the MEP pathway (Fig. 7A; see also Table S1 and Fig. S5). Hierarchical clustering indicates that resistant clones are characterized by a metabolic signature of increased levels of FBP (fructose 1,6-bisphosphatase), DOXP, and MEcPP (Fig. 7A). We observed that the levels of abundance of DOXP and MEcPP are tightly correlated with cellular levels of the PFK9 product, FBP (Fig. 7B) ($P < 0.01$), but not with those of the other upstream glycolytic metabolites, such as glu6P/fru6P (Fig. 7C) ($P > 0.2$).

Of note, the *pfk9*^{T1206I} suppressor allele in strains S1 and S2 restored nearly parental levels of FBP and downstream MEP pathway intermediates (Fig. 7A), consistent with our finding that PFK activity was reduced in lysate from these strains (Fig. 6B).

DISCUSSION

Cells must control levels of critical metabolites in order to efficiently utilize carbon sources for energy and biosynthesis of essential molecules. Cells may regulate their metabolism via transcriptional, posttranscriptional, posttranslational, allosteric, or enzymatic mechanisms that are necessary for growth (57–60). In the glucose-rich red blood cell niche, *Plasmodium* malaria parasites display a unique dependence on glycolysis for energy and biosynthesis.

Using resistance to a metabolic inhibitor, we identified a phosphatase member of the HAD superfamily, HAD2, as a novel regulator of metabolism in *P. falciparum*. Importantly, HAD2 controls substrate availability to the parasite-specific MEP pathway for synthesis of isoprenoids, which are promising drug targets for much needed new antimalarials. We found that tolerance of inhibitors such as FSM is a robust and sensitive readout of metabolic perturbation. HAD2 is necessary for metabolic homeostasis in malaria parasites. Cells lacking HAD2 exhibit marked dysregulation of central carbon metabolism, including altered steady-state levels of glycolytic intermediates and isoprenoid precursors. We found that mutations in phosphofructokinase (*PFK9*) restored wild-type growth rates and FSM sensitivity to our *had2* mutant strains. Our report thus genetically connects the function of HAD2, a HAD superfamily member, to control of essential central carbon metabolism. In addition, our work revealed a previously undescribed strategy by which malaria parasites may respond to cellular metabolic dysregulation through mutation in the gene encoding the rate-limiting glycolytic enzyme PFK9.

HAD2 is a member of the HAD superfamily and a homolog of the previously described metabolic regulator HAD1. Together with our previous studies on HAD1 (20, 21), we define the cellular role of these proteins in *P. falciparum* and contribute to the greater understanding of the HADs, an evolutionarily conserved and widespread protein family. Both enzymes belong to the IIB (IPR006379) and Cof-like hydrolase (IPR000150) subfamilies (22). HAD enzymes display diverse substrate preferences (23, 27, 43, 44, 61–64), and their biological functions are largely unknown. Like other HAD homologs, including PfHAD1 (20), HAD2 appears to be a cytoplasmic phosphatase with a preference for small, monophosphorylated substrates. While the HAD superfamily is thought to consist of a highly evolvable pool of enzymes with broad substrate specificity (37, 42), our work strongly suggests that, like HAD1 and HAD2, other members of this superfamily are likely to perform specific and biologically important cellular functions.

We found that HAD1 and HAD2 influence central carbon metabolism. In our studies of fosmidomycin resistance, we were uniquely positioned to detect these related but distinct mechanisms of metabolic regulation through the study of the MEP pathway, whose substrate availability is closely linked to glycolysis. *had2* mutations were found at a lower rate than *had1* mutations (20) and appeared to have a fitness cost in FSM^r parasites, suggesting that, despite their homology, HAD1 and HAD2 have distinct metabolic roles *in vivo*. As has been suggested by others in the HAD field (42, 65, 66), HADs are amenable to evolution of their substrate specificity and may quickly adopt divergent cellular functions, which may result in different fitness phenotypes upon mutation.

The exact mechanism by which HAD2 enacts its regulation on parasite glycolysis remains unclear. Possible mechanisms include direct or indirect regulation of PFK9 by HAD2, as well as HAD2-mediated regulation of glycolysis downstream of PFK9, such that mutation of *PFK9* is a "bypass" mechanism in *had2* mutants (Fig. 8). HAD2 itself may also be subject to regulation, and understanding this regulation may be key in uncovering HAD2's *in vivo* function and mechanism of glycolytic regulation. HAD2 from *P. vivax* is sensitive to inhibition by free phosphate (40), which may influence its *in vivo* substrate specificity in a cellular context. PfHAD2 has also appears to be phosphorylated *in vivo* (67, 68), and changes in phosphorylation often greatly influence enzymatic activity *in vivo*. As *P. falciparum* has a smaller repertoire of HADs than bacterial species
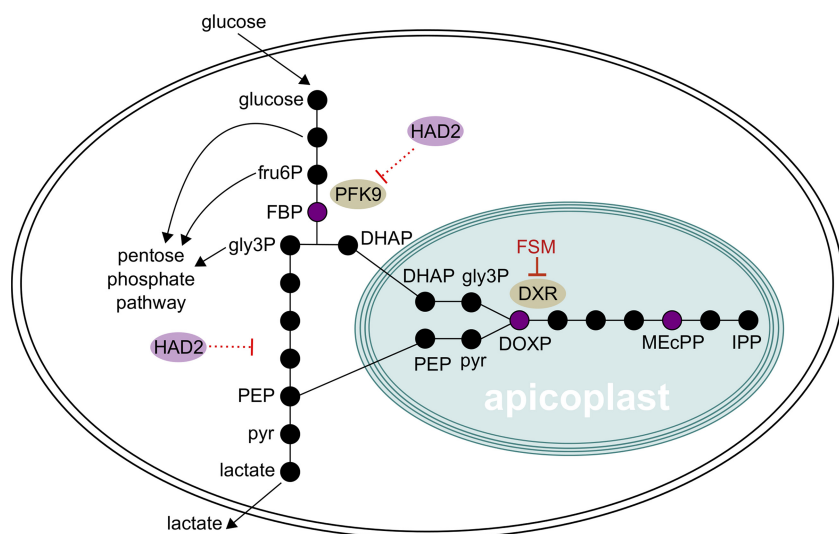
FIG 8 Model of HAD2- and PFK9-mediated metabolic regulation. Abbreviations: fru6P, fructose 6-phosphate; FBP, fructose 1,6-bisphosphate; gly3P, glyceraldehyde 3-phosphate; DHAP, dihydroxyacetone phosphate; pyr, pyruvate; PEP, phosphoenolpyruvate; DOXP, deoxyxylulose 5-phosphate, MEcPP, 2-C-methyl-D-erythritol 2,4-cyclodiphosphate; IPP, isopentenyl pyrophosphate. Black circles represent metabolites. Key metabolites (FBP, DOXP, and MEcPP) are shown in purple. The glycolytic metabolites DHAP and PEP are imported into the apicoplast and are converted to gly3P and pyruvate, respectively (89, 90). HAD2 may act as a negative regulator of PFK9, directly or indirectly, or may inhibit glycolysis downstream of PFK9. Loss of HAD2 results in increased substrate availability to the MEP pathway. In *had2* strains, reduction in PFK9 activity may counteract or bypass metabolic perturbations due to loss of HAD2.

and *Plasmodium* HADs influence easily quantified phenotypes (drug tolerance, growth, metabolite levels), the malaria parasite may be an attractive system for study of the molecular mechanisms by which HAD proteins control metabolic homeostasis and growth.

Metabolic profiling reveals that loss of HAD2 function leads to metabolic dysregulation, which is centered on the canonical rate-limiting step of glycolysis, catalyzed by PFK9. While the cellular abundance of the PFK9 product FBP is increased in *had2* parasites, HAD2 does not directly utilize FBP as an enzymatic substrate, suggesting an indirect mechanism of HAD2-mediated metabolic regulation. However, the distinct metabolic signature of *had2* parasites, characterized by increased levels of the MEP pathway metabolites DOXP and MEcPP and the key glycolytic metabolite FBP, suggests that MEP pathway metabolism is precisely linked to FBP production. In other microbial systems, FBP levels reflect metabolic flux and are cued to environmental perturbations (69). FBP-centered metabolic regulation is also important for the related apicomplexan *Toxoplasma gondii*, which constitutively expresses fructose 1,6-bisphosphatase (FBPase) to fine-tune glucose metabolism (57). While *P. falciparum* does not appear to possess an FBPase (necessary for gluconeogenesis), the parasite may possess alternative FBP-sensing mechanisms to tune metabolism, perhaps via regulators such as HAD1 and HAD2.

The metabolic dysregulation that we have observed in the *had2* mutant strains appears to be associated with a fitness disadvantage. Under conditions of FSM selective pressure, the benefits of dysregulated metabolism outweigh the costs. However, in the absence of FSM, *had2* parasites achieve metabolic relief through secondary mutation in *PFK9*. The improved growth of *had2 pfk9* double mutant parasites, compared to parasites with a *had2* single mutation, argues that the growth and metabolic phenotypes are linked. However, our complementation studies cannot strictly discern whether restoring HAD2 directly increases the growth rate of the *had2* strain, as transfection and complementation of HAD2 inherently constitute additional selection for increased fitness. Of note, two recent essentiality screens performed in *Plasmodium* spp. found that HAD2 is dispensable for growth and that loss of HAD2 was not

associated with any significant fitness defect (70, 71). However, it is unknown whether the mutant strains generated in these screens have also acquired additional suppressor mutations, such as polymorphisms in *PFK9*, that have facilitated their growth.

Likewise, *PFK9* provides an additional case study of the context dependence of gene essentiality in *Plasmodium* spp. Given its involvement in the canonical rate-limiting step in glycolysis, *PFK9* is strongly predicted to be essential for asexual growth of malaria parasites (70, 71). In the context of a *had2* mutation, our strains readily develop mutations in *PFK9* that reduce function but are nonetheless associated with increased fitness. Indeed, it is surprising that parasites that are entirely dependent on glycolysis for ATP production tolerate such a significant loss of activity in this enzyme. Because we identified mutations across the length of *PFK9* in our suppressed strains, our studies do not appear to point to a specific disrupted function, such as alterations in an allosteric binding pocket or a dimer interface. The observed mutability of *PFK9* points to a remarkable and unexpected metabolic plasticity in the parasite. That is, even though the parasite inhabits a highly controlled intraerythrocytic niche, a wide range of metabolic states of *P. falciparum* growth are still permissive for parasite growth. This previously undescribed metabolic plasticity centered on PFK9 should be considered in future efforts to target essential metabolism in *Plasmodium*.

Combined with the study described above, our work highlights the central role of the glycolytic enzyme PFK9. A recent kinetic model of parasite glycolysis confirms that PFK has a high flux-control coefficient, is sensitive to competitive inhibition, and can effectively reduce glycolytic flux (72, 73). Like HAD, PFK9 is plant-like and evolutionarily divergent from its mammalian homologs (51). These differences may be exploited for PFK inhibitor design and may indicate that PFK9 can be specifically targeted for antimalarial development. However, our work cautions that the parasite has a surprising capacity to adapt to perturbations in central carbon metabolism, which may present challenges in targeting these pathways.

Finally, our approach demonstrates the power of forward genetics to uncover novel biology in a clinically relevant, non-model organism. We employ a previously described screen (20) to uncover a novel resistance locus and employ a second selection for parasite fitness to identify changes that suppress our resistance phenotype. Of the 19 strains in our original FSM resistance screen (20), we identified only one *had2* mutant, likely due to the reduced fitness associated with resistance in this strain. While fitness costs associated with antimalarial resistance are well known (74–77), this study represents, to our knowledge, the first to harness this evolutionary trade-off to identify suppressor mutations in a nontarget locus. Additional methods to identify low-fitness resistant mutants have recently been recently described (77), and fitness assessment of resistance mutations may allow suppressor screening for other antimalarials or other target pathways to reveal new aspects of biology and drug resistance in malaria parasites.

MATERIALS AND METHODS

Parasite strains and culture. Unless otherwise indicated, parasites were maintained at 37°C in 5% O_2–5% CO_2–90% N_2 in a 2% suspension of human erythrocytes in RPMI medium (Sigma-Aldrich) modified with 27 mM $NaHCO_3$, 11 mM glucose, 5 mM HEPES, 0.01 mM thymidine, 1 mM sodium pyruvate, 0.37 mM hypoxanthine, 10 μg/ml gentamicin, and 5 g/liter Albumax (Thermo Fisher Scientific).

FSM^r strain E2 was generated by selecting a clone of genome reference strain 3D7 (MRA-102 from MR4; ATCC, Manassas, VA) under conditions of continuous treatment with 3 μM FSM, as previously described (20). Clones of strain E2 were isolated by limiting dilution.

Quantification of FSM resistance. Opaque 96-well plates were seeded with asynchronous cultures at 0.5% to 1.0% parasitemia (percentage of infected red blood cells). After 3 days, media were removed and parasitemia was measured via Picogreen fluorescence on a POLARStar Omega spectrophotometer (BMG Labtech), as previously described (78). Half-maximal inhibitory concentration (IC_{50}) values were calculated using GraphPad Prism. Unless otherwise indicated, all IC_{50} data are representative of means of results from ≥3 independent experiments performed with technical replicates.

HAD2 structural alignment. Structures were aligned using the TM-align algorithm in Lasergene Protean 3D software (root mean square deviation [RMSD] of 1.9 Å).

Whole-genome sequencing and variant analysis. Library preparation, sequencing, read alignment, and variant analyses were performed by the Washington University Genome Technology Access Center. One microgram of parasite genomic DNA was sheared, end repaired, and adapter ligated. Libraries were

sequenced on an Illumina HiSeq 2500 system in Rapid Run mode to generate 101-bp paired-end reads. Reads were aligned to the *P. falciparum* 3D7 reference genome (PlasmoDB v7.2) using Novoalign (V2.08.02). Duplicate reads were removed. SNPs were called using samtools (quality score of ≥20, read depth of ≥5) and annotated using snpEff. Background variants were removed using previously sequenced genomes from parental and control strains (20). Mixed-variant calls and variants in highly variable surface antigen loci (79, 80) were removed.

Sanger sequencing. The *HAD2* (PlasmoDB PF3D7_1226300) A469T (R157X) SNP was amplified and sequenced using the HAD2_R157X_F and HAD2_R157X_R primers. The *PFK9* locus was amplified using the PFK9_F and PFK9_R primers. *PFK9* amplicons were sequenced using the PFK9_seq (1–8) primers. Primer sequences can be found in Table S2 in the supplemental material.

Generation of recombinant HAD2. The predicted coding sequence of *HAD2* was amplified using the HAD2_LIC_F and HAD2_LIC_R primers (Table S2). A catalytic mutant (D26A) was also generated to use as a negative control in activity assays. The *had2^D26A^* allele was created using the HAD2_D26A_F and HAD2_D26A_R site-directed mutagenesis primers (Table S2).

Ligation-independent cloning was used to clone *HAD2* and *had2^D26A^* into vector BG1861 (81), which introduces an N-terminal 6×His fusion into the expressed protein. BG1861:6×His-HAD2 was transformed into One Shot BL21(DE3)pLysS *Escherichia coli* cells (Thermo Fisher Scientific). Protein expression was induced for 3 h with 1 mM isopropyl-β-D-thiogalactoside at mid-log phase (optical density at 600 nm [OD_{600}] of 0.4 to 0.5). Cells were collected by centrifugation and stored at −20°C.

Cells were lysed in buffer containing 1 mg/ml lysozyme, 20 mM imidazole, 1 mM dithiothreitol, 1 mM $MgCl_2$ 10 mM Tris HCl (pH 7.5), 30 U benzonase (EMD Millipore), and EDTA-free protease inhibitor tablets (Roche). 6×His-HAD2 was bound to nickel agarose beads (Gold Biotechnology), washed with a mixture containing 20 mM imidazole, 20 mM Tris HCl (pH 7.5), and 150 mM NaCl, and eluted in a mixture containing 300 mM imidazole, 20 mM Tris HCl (pH 7.5), and 150 mM NaCl. This eluate was further purified by size exclusion gel chromatography using a HiLoad 16/600 Superdex 200-pg column (GE Healthcare) equilibrated in a mixture containing 25 mM Tris HCl (pH 7.5), 250 mM NaCl, and 1 mM $MgCl_2$. The elution fractions containing HAD2 were pooled and concentrated, and glycerol was added to reach a concentration of 10% (wt/vol). Protein solutions were immediately flash frozen and stored at −80°C.

HAD2 activity assays. The rate of *para*-nitrophenyl phosphate (*p*NPP; Sigma-Aldrich S0942) hydrolysis by HAD2 was determined by continuous measurement of absorbance at 405 nm. Assays were performed at 37°C in a 50-μl volume consisting of 50 mM Tris-HCl (pH 7.5), 5 mM $MgCl_2$, 10 mM *p*NPP, and 1.2 μM enzyme.

Hydrolysis of other phosphorylated substrates by HAD2 was measured using an EnzChek phosphate assay kit (Life Technologies). The reaction buffer was modified to contain 50 mM Tris-HCl (pH 8.0), 20 mM $MgCl_2$, 0.2 mM 2-amino-6-mercapto-7-methylpurine riboside (MESG), and 1 U/ml purine nucleoside phosphorylase (PNP). Reaction mixtures contained 5 mM substrate and 730 nM enzyme. The activity of catalytically inactive 6×His-HAD2^D26A^ was measured for all substrates, and the data were used to normalize the activity found for the WT HAD2 enzyme. Activity was normalized to that obtained from catalytically inactive 6×His-HAD2^D26A^. All data represent means of results from ≥3 independent experiments performed with technical replicates.

***P. falciparum* growth assays.** Asynchronous cultures were seeded at 1% parasitemia. Media (no drug) were exchanged daily. Samples were taken at indicated time points and fixed in phosphate-buffered saline (PBS)–4% paraformaldehyde–0.05% glutaraldehyde. Cells were stained with 0.01 mg/ml acridine orange, and parasitemia was determined on a BD Biosciences LSRII flow cytometer (Thermo Fisher Scientific). All data represent means of results from ≥3 independent experiments.

pTEOE110:HAD2 plasmid construction. The pTEOE110 construct contains the heat shock protein 110 gene (PF3D7_0708800) 5′ untranscribed region (UTR) and a C-terminal GFP tag (20). Human dihydrofolate reductase (hDHFR) is present as a selectable marker. Inverted terminal repeats are included for genome integration by a cotransfected piggyBac transposase (pHTH, MRA-912 from MR4; ATCC, Manassas, VA).

HAD2 was amplified with the HAD2_XhoI_F and HAD2_AvrII_R primers (Table S2) and cloned into AvrII and XhoI sites in the pTEOE110 plasmid.

Parasite transfections. Transfections were performed as previously described (20). Briefly, 50 to 100 μg of plasmid DNA was precipitated and resuspended in Cytomix (25 mM HEPES [pH 7.6], 120 mM KCl, 0.15 mM $CaCl_2$, 2 mM EGTA, 5 mM $MgCl_2$, 10 mM K_2HPO_4).

A ring-stage *P. falciparum* culture was washed with Cytomix and resuspended in the DNA/Cytomix solution. Cells were electroporated using a Bio-Rad Gene Pulser II electroporator at 950 μF and 0.31 kV. Electroporated cells were washed with media and returned to normal culture conditions. Parasites expressing the construct were selected by continuous treatment with 5 nM WR92210 (Jacobus Pharmaceuticals). Transfectants were cloned by limiting dilution, and the presence of the HAD2-GFP construct was verified by PCR using gene- and GFP-specific primers (HAD2_R157X_F and GFP_R; Table S2). Maintenance of the endogenous *HAD2* and *PFK9* genotypes was verified by Sanger sequencing.

Antiserum generation. Polyclonal anti-HAD2 antiserum was raised against 6×His-HAD2 in rabbits, with TiterMax as an adjuvant (Cocalico Biologicals). Antiserum specificity was confirmed by immunoblotting of lysate lacking HAD2. Polyclonal anti-HAD1 antiserum was previously described (MRA-1256 from MR4; ATCC) (20).

Immunoblotting. Lysates were separated on a polyacrylamide gel and transferred to a polyvinylidene difluoride membrane. Membranes were blocked in 5% nonfat dry milk–0.1% Tween 20–PBS. Rabbit polyclonal antisera were used at the following dilutions: 1:2,000 to 5,000 anti-HAD2 and 1:20,000 anti-HAD1 (20). For all blots, 1:20,000 horseradish peroxidase (HRP)-conjugated goat anti-rabbit IgG

antibody was used as a secondary antibody (ThermoFisher 65-6120). Blots were stripped with 200 mM glycine–0.1% SDS–1% Tween 20 (pH 2.2) and reprobed with 1:5,000 rabbit anti-heat shock protein 70 (Hsp70) (AS08 371; Agrisera Antibodies) as a loading control. All blots shown are representative of results from ≥3 independent experiments. Minimal adjustments were applied equally to all blot images.

PfPFK model construction. PfPFK subunits were searched against the HHpred server for protein remote homology detection and three-dimensional (3D) structure prediction using statistics as previously described (82–85). The *Borellia burgdorferi* PFK structure (PDB 1KZH) (86) returned the highest similarity for both PfPFK domains and was used to predict the 3D structure for each domain using the program MODELLER. PFK product orientation in the active site of the model was predicted via the alignment tool, using PyMOL software against the *E. coli* PFK crystal structure (PDB 1PFK) (87). The α domain model encompasses amino acids 779 to 1347, and the β domain model encompasses amino acids 110 to 638.

Assay of native PFK9 activity. Sorbitol-synchronized trophozites were isolated using 0.1% saponin. Cells were washed in buffer containing 100 mM Tris-HCl (pH 7.5), 1 mM MgCl$_2$, 1 mM dithiothreitol (DTT), 10% glycerol, and EDTA-free protease inhibitor tablets (Roche) and lysed by sonication at 4°C (Fisher Scientific model 550 Sonic Dismembrator; amplitude of 3.5), followed by centrifugation at 4°C (10,000 × g, 10 min). An "RBC carryover" control was comprised of the trace cellular material remaining after saponin lysis, centrifugation, and washing of uninfected erythrocytes.

Lysate PFK9 activity was monitored by linking it to the oxidation of NADH, as previously described (51, 56). Reaction mixtures contained 100 mM Tris-HCl (pH 7.5), 1 mM MgCl$_2$, 1 mM DTT, 0.25 mM NADH, 1 mM ATP, 3 mM fructose 6-phosphate, and excess volumes of linking enzymes aldolase (7.5 U), triose-phosphate isomerase (3.8 U), and glycerol 3-phosphate dehydrogenase (3.8 U). After fresh cell lysate (10 to 15 μg total protein) was added, absorbance at 340 nm was measured at 37°C for 40 min. Activity was determined by linear regression using GraphPad Prism software. Unless otherwise indicated, data represent means of results from ≥3 independent experiments.

Metabolite profiling. Approximately ~1 × 10^9 sorbitol-synchronized early trophozites were isolated using 0.1% saponin, washed with ice-cold PBS–2 g/liter glucose, and frozen at −80°C. Samples were extracted in 600 μl of ice-cold extraction solvent (chloroform, methanol, and acetonitrile [2:1:1 {vol/vol/vol}]) using two liquid-nitrogen-cooled 3.2-mm-diameter stainless steel beads and homogenization in a Tissue-Lyser II instrument (Qiagen) at 20 Hz for 5 min in a cold sample rack. Ice-cold water was added, and samples were homogenized for 5 min at 20 Hz. Samples were centrifuged at 14,000 relative centrifugal force (rcf) at 4°C for 5 min. The polar phase was lyophilized and redissolved in 100 μl water and analyzed by liquid chromatography-tandem mass spectrometry (LC-MS/MS). LC-MS/MS was performed on a 4000QTRAP system (AB Sciex) in multiple-reaction monitoring mode using negative ioniziation and 10 mM tributylammonium acetate (pH 5.1 to 5.5) as the ion pair reagent. The specific parameters used for analysis of MEP pathway metabolites have been previously described (19). Liquid chromatography separation was performed using ion pair reverse-phase chromatography (88) with the following modifications: (i) RP-hydro high-performance liquid chromatography column (Phenomenex) (100 mm by 2.0 mm, 2.5-μm pore size); (ii) flow rate of 0.14 ml/min; (iii) solvent A, consisting of 10 mM tributylammonium acetate–5% methanol; (iv) binary LC gradient (20% solvent B [100% methanol] from 0 to 2.5 min, 30% solvent B for 12.5 min, 80% solvent B for 5 min, and column equilibration at for 5 min); and (v) a 20-μl autosampler injection volume.

Additional methods. Additional methods are provided in Text S1 in the supplemental material.

Accession number(s). All genome data have been deposited in the NCBI BioProject database (PRJNA222697) and Sequence Read Archive (SRP038937).

SUPPLEMENTAL MATERIAL

Supplemental material for this article may be found at https://doi.org/10.1128/mBio .01193-18.

TEXT S1, DOCX file, 0.02 MB.

FIG S1, TIF file, 0.4 MB.

FIG S2, TIF file, 0.2 MB.

FIG S3, TIF file, 2.4 MB.

FIG S4, TIF file, 0.8 MB.

FIG S5, TIF file, 0.5 MB.

TABLE S1, DOCX file, 0.02 MB.

TABLE S2, DOCX file, 0.02 MB.

DATA SET S1, PDF file, 0.2 MB.

ACKNOWLEDGMENTS

REFERENCES

1. World Health Organization. 2017. World Malaria Report 2017. WHO, Geneva, Switzerland.

2. Dondorp AM, Nosten F, Yi P, Das D, Phyo AP, Tarning J, Lwin KM, Ariey F, Hanpithakpong W, Lee SJ, Ringwald P, Silamut K, Imwong M, Chotivanich K, Lim P, Herdman T, An SS, Yeung S, Singhasivanon P, Day NPJ, Lindegardh N, Socheat D, White NJ. 2009. Artemisinin resistance in *Plasmodium falciparum* malaria. N Engl J Med 361:455–467. https://doi.org/10.1056/NEJMoa0808859.

3. Ashley EA, Dhorda M, Fairhurst RM, Amaratunga C, Lim P, Suon S, Sreng S, Anderson JM, Mao S, Sam B, Sopha C, Chuor CM, Nguon C, Sovann-aroth S, Pukrittayakamee S, Jittamala P, Chotivanich K, Chutasmit K, Suchatsoonthorn C, Runcharoen R, Hien TT, Thuy-Nhien NT, Thanh NV, Phu NH, Htut Y, Han K-T, Aye KH, Mokuolu OA, Olaosebikan RR, Folaranmi OO, Mayxay M, Khanthavong M, Hongvanthong B, Newton PN, Onyamboko MA, Fanello CI, Tshefu AK, Mishra N, Valecha N, Phyo AP, Nosten F, Yi P, Tripura R, Borrmann S, Bashraheil M, Peshu J, Faiz MA, Ghose A, Hossain MA, Samad R, et al. 2014. Spread of artemisinin resistance in *Plasmodium falciparum* malaria. N Engl J Med 371:411–423. https://doi.org/10.1056/NEJMoa1314981.

4. Mehta M, Sonawat HM, Sharma S. 2006. Glycolysis in *Plasmodium falciparum* results in modulation of host enzyme activities. J Vector Borne Dis 43:95–103.

5. Roth E. 1990. *Plasmodium falciparum* carbohydrate metabolism: a connection between host cell and parasite. Blood Cells 16:453–466.

6. Roth EF. 1987. Malarial parasite hexokinase and hexokinase-dependent glutathione reduction in the *Plasmodium falciparum*-infected human erythrocyte. J Biol Chem 262:15678–15682.

7. Bowman IB, Grant PT, Kermack WO, Ogston D. 1961. The metabolism of *Plasmodium berghei*, the malaria parasite of rodents. 2. An effect of mepacrine on the metabolism of glucose by the parasite separated from its host cell. Biochem J 78:472–478. https://doi.org/10.1042/bj0780472.

8. Krungkrai J, Burat D, Kudan S, Krungkrai S, Prapunwattana P. 1999. Mitochondrial oxygen consumption in asexual and sexual blood stages of the human malarial parasite, *Plasmodium falciparum*. Southeast Asian J Trop Med Public Health 30:636–642.

9. MacRae JI, Dixon MW, Dearnley MK, Chua HH, Chambers JM, Kenny S, Bottova I, Tilley L, McConville MJ. 2013. Mitochondrial metabolism of sexual and asexual blood stages of the malaria parasite *Plasmodium falciparum*. BMC Biol 11:67. https://doi.org/10.1186/1741-7007-11-67.

10. Scheibel LW, Miller J. 1969. Glycolytic and cytochrome oxidase activity in Plasmodia. Mil Med 134:1074–1080. https://doi.org/10.1093/milmed/134.9.1074.

11. Gershenzon J, Dudareva N. 2007. The function of terpene natural products in the natural world. Nat Chem Biol 3:408–414. https://doi.org/10.1038/nchembio.2007.5.

12. Guggisberg AM, Amthor RE, Odom AR. 2014. Isoprenoid biosynthesis in *Plasmodium falciparum*. Eukaryot Cell 13:1348–1359. https://doi.org/10.1128/EC.00160-14.

13. Imlay L, Odom AR. 2014. Isoprenoid metabolism in apicomplexan parasites. Curr Clin Microbiol Rep 1:37–50. https://doi.org/10.1007/s40588-014-0006-7.

14. Jordão FM, Kimura EA, Katzin AM. 2011. Isoprenoid biosynthesis in the erythrocytic stages of *Plasmodium falciparum*. Mem Inst Oswaldo Cruz 106:134–141. https://doi.org/10.1590/S0074-02762011000900018.

15. Lange BM, Rujan T, Martin W, Croteau R. 2000. Isoprenoid biosynthesis: the evolution of two ancient and distinct pathways across genomes. Proc Natl Acad Sci U S A 97:13172–13177. https://doi.org/10.1073/pnas.240454797.

16. Koppisch AT, Fox DT, Blagg BSJ, Poulter CD. 2002. *E. coli* MEP synthase: steady-state kinetic analysis and substrate binding. Biochemistry 41:236–243. https://doi.org/10.1021/bi0118207.

17. Kuzuyama T, Shimizu T, Takahashi S, Seto H. 1998. Fosmidomycin, a specific inhibitor of 1-deoxy-d-xylulose 5-phosphate reductoisomerase in the nonmevalonate pathway for terpenoid biosynthesis. Tetrahedron Lett 39:7913–7916. https://doi.org/10.1016/S0040-4039(98)01755-9.

18. Steinbacher S, Kaiser J, Eisenreich W, Huber R, Bacher A, Rohdich F. 2003. Structural basis of fosmidomycin action revealed by the complex with 2-C-methyl-D-erythritol 4-phosphate synthase (IspC). Implications for the catalytic mechanism and anti-malaria drug development. J Biol Chem 278:18401–18407. https://doi.org/10.1074/jbc.M300993200.

19. Zhang B, Watts KM, Hodge D, Kemp LM, Hunstad DA, Hicks LM, Odom AR. 2011. A second target of the antimalarial and antibacterial agent fosmidomycin revealed by cellular metabolic profiling. Biochemistry 50:3570–3577. https://doi.org/10.1021/bi200113y.

20. Guggisberg AM, Park J, Edwards RL, Kelly ML, Hodge DM, Tolia NH, Odom AR. 2014. A sugar phosphatase regulates the methylerythritol phosphate (MEP) pathway in malaria parasites. Nat Commun 5:4467. https://doi.org/10.1038/ncomms5467.

21. Park J, Guggisberg AM, Odom AR, Tolia NH. 2015. Cap-domain closure enables diverse substrate recognition by the C2-type haloacid dehalogenase-like sugar phosphatase *Plasmodium falciparum* HAD1. Acta Crystallogr D Biol Crystallogr 71:1824–1834. https://doi.org/10.1107/S1399004715012067.

22. Hunter S, Jones P, Mitchell A, Apweiler R, Attwood TK, Bateman A, Bernard T, Binns D, Bork P, Burge S, de Castro E, Coggill P, Corbett M, Das U, Daugherty L, Duquenne L, Finn RD, Fraser M, Gough J, Haft D, Hulo N, Kahn D, Kelly E, Letunic I, Lonsdale D, Lopez R, Madera M, Maslen J, McAnulla C, McDowall J, McMenamin C, Mi H, Mutowo-Muellenet P, Mulder N, Natale D, Orengo C, Pesseat S, Punta M, Quinn AF, Rivoire C, Sangrador-Vegas A, Selengut JD, Sigrist CJA, Scheremetjew M, Tate J, Thimmajanarthanan M, Thomas PD, Wu CH, Yeats C, Yong S-Y. 2012. InterPro in 2011: new developments in the family and domain prediction database. Nucleic Acids Res 40:D306–D312. https://doi.org/10.1093/nar/gkr948.

23. Kuznetsova E, Proudfoot M, Gonzalez CF, Brown G, Omelchenko MV, Borozan I, Carmel L, Wolf YI, Mori H, Savchenko AV, Arrowsmith CH, Koonin EV, Edwards AM, Yakunin AF. 2006. Genome-wide analysis of substrate specificities of the *Escherichia coli* haloacid dehalogenase-like phosphatase family. J Biol Chem 281:36149–36161. https://doi.org/10.1074/jbc.M605449200.

24. Kang MJ, Lee YM, Yoon SH, Kim JH, Ock SW, Jung KH, Shin YC, Keasling JD, Kim SW. 2005. Identification of genes affecting lycopene accumulation in *Escherichia coli* using a shot-gun method. Biotechnol Bioeng 91:636–642. https://doi.org/10.1002/bit.20539.

25. Kang Y, Weber KD, Qiu Y, Kiley PJ, Blattner FR. 2005. Genome-wide expression analysis indicates that FNR of *Escherichia coli* K-12 regulates a large number of genes of unknown function. J Bacteriol 187:1135–1160. https://doi.org/10.1128/JB.187.3.1135-1160.2005.

26. Pratish G, Radhakrishnan M. 2014. Engineering *Escherichia coli* for D-ribose production from glucose-xylose mixtures. Ind Biotechnol 10:106–114.

27. Roberts A, Lee S-Y, McCullagh E, Silversmith RE, Wemmer DE. 2005. YbiV

from *Escherichia coli* K12 is a HAD phosphatase. Proteins 58:790–801. https://doi.org/10.1002/prot.20267.

28. Sun Y, Vanderpool CK. 2013. Physiological consequences of multiple-target regulation by the small RNA SgrS in *Escherichia coli*. J Bacteriol 195:4804–4815. https://doi.org/10.1128/JB.00722-13.

29. Guggisberg AM, Frasse PM, Jezewski AJ, Kafai NM, Gandhi AY, Erlinger SJ, Odom John AR. 2018. Suppression of drug resistance reveals a genetic mechanism of metabolic plasticity in malaria parasites. bioRxiv https://doi.org/10.1101/155523.

30. Yeh E, DeRisi JL. 2011. Chemical rescue of malaria parasites lacking an apicoplast defines organelle function in blood-stage *Plasmodium falciparum*. PLoS Biol 9:e1001138. https://doi.org/10.1371/journal.pbio.1001138.

31. Jomaa H, Wiesner J, Sanderbrand S, Altincicek B, Weidemeyer C, Hintz M, Türbachova I, Eberl M, Zeidler J, Lichtenthaler HK, Soldati D, Beck E. 1999. Inhibitors of the nonmevalonate pathway of isoprenoid biosynthesis as antimalarial drugs. Science 285:1573–1576. https://doi.org/10.1126/science.285.5433.1573.

32. Estévez JM, Cantero A, Reindl A, Reichler S, León P. 2001. 1-Deoxy-D-xylulose-5-phosphate synthase, a limiting enzyme for plastidic isoprenoid biosynthesis in plants. J Biol Chem 276:22901–22909. https://doi.org/10.1074/jbc.M100854200.

33. Mahmoud SS, Croteau RB. 2001. Metabolic engineering of essential oil yield and composition in mint by altering expression of deoxyxylulose phosphate reductoisomerase and menthofuran synthase. Proc Natl Acad Sci U S A 98:8915–8920. https://doi.org/10.1073/pnas.141237298.

34. Carretero-Paulet L, Cairó A, Botella-Pavía P, Besumbes O, Campos N, Boronat A, Rodríguez-Concepción M. 2006. Enhanced flux through the methylerythritol 4-phosphate pathway in *Arabidopsis* plants overexpressing deoxyxylulose 5-phosphate reductoisomerase. Plant Mol Biol 62:683–695. https://doi.org/10.1007/s11103-006-9051-9.

35. Morrone D, Lowry L, Determan MK, Hershey DM, Xu M, Peters RJ. 2010. Increasing diterpene yield with a modular metabolic engineering system in *E. coli*: comparison of MEV and MEP isoprenoid precursor pathway engineering. Appl Microbiol Biotechnol 85:1893–1906. https://doi.org/10.1007/s00253-009-2219-x.

36. Aurrecoechea C, Brestelli J, Brunk BP, Dommer J, Fischer S, Gajria B, Gao X, Gingle A, Grant G, Harb OS, Heiges M, Innamorato F, Iodice J, Kissinger JC, Kraemer E, Li W, Miller JA, Nayak V, Pennington C, Pinney DF, Roos DS, Ross C, Stoeckert CJ, Treatman C, Wang H. 2009. PlasmoDB: a functional genomic database for malaria parasites. Nucleic Acids Res 37:D539–D543. https://doi.org/10.1093/nar/gkn814.

37. Burroughs AM, Allen KN, Dunaway-Mariano D, Aravind L. 2006. Evolutionary genomics of the HAD superfamily: understanding the structural adaptations and catalytic diversity in a superfamily of phosphoesterases and allied enzymes. J Mol Biol 361:1003–1034. https://doi.org/10.1016/j.jmb.2006.06.049.

38. Koonin EV, Tatusov RL. 1994. Computer analysis of bacterial haloacid dehalogenases defines a large superfamily of hydrolases with diverse specificity. Application of an iterative approach to database search. J Mol Biol 244:125–132. https://doi.org/10.1006/jmbi.1994.1711.

39. Aravind L, Galperin MY, Koonin EV. 1998. The catalytic domain of the P-type ATPase has the haloacid dehalogenase fold. Trends Biochem Sci 23:127–129. https://doi.org/10.1016/S0968-0004(98)01189-X.

40. Srinivasan B, Kempaiah Nagappa L, Shukla A, Balaram H. 2015. Prediction of substrate specificity and preliminary kinetic characterization of the hypothetical protein PVX_123945 from *Plasmodium vivax*. Exp Parasitol 151-152:56–63. https://doi.org/10.1016/j.exppara.2015.01.013.

41. Kuznetsova E, Proudfoot M, Sanders SA, Reinking J, Savchenko A, Arrowsmith CH, Edwards AM, Yakunin AF. 2005. Enzyme genomics: application of general enzymatic screens to discover new enzymes. FEMS Microbiol Rev 29:263–279. https://doi.org/10.1016/j.fmrre.2004.12.006.

42. Kuznetsova E, Nocek B, Brown G, Makarova KS, Flick R, Wolf YI, Khusnutdinova A, Evdokimova E, Jin K, Tan K, Hanson AD, Hasnain G, Zallot R, de Crécy-Lagard V, Babu M, Savchenko A, Joachimiak A, Edwards AM, Koonin EV, Yakunin AF. 2015. Functional diversity of haloacid dehalogenase superfamily phosphatases from *Saccharomyces cerevisiae*: biochemical, structural, and evolutionary insights. J Biol Chem 290:18678–18698. https://doi.org/10.1074/jbc.M115.657916.

43. Titz B, Häuser R, Engelbrecher A, Uetz P, Alatossava T, Jutte H, Kuhn A, Kellenberger E, Aravind L, Koonin EV, Baba T, Ara T, Hasegawa M, Takai Y, Okumura Y, Baba M, Datsenko KA, Tomita M, Wanner BL, Mori H, Bacon DF, Treffers HP, Bateman A, Coin L, Durbin R, Baykov AA, Evtushenko OA, Avaeva SM, Bessman MJ, Frick DN, O'Handley SF, Cohen SS,

44. Flaks JG, Barner HD, Loeb MR, Lichtenstein J, Cox EC, Yanofsky C, Datsenko KA, Wanner BL, Galperin MY, Moroz OV, Wilson KS, Murzin AG, Guzman LM, Belin D, Carson MJ, Beckwith J, Harbers E, Chaudhuri NK, et al. 2007. The *Escherichia coli* protein YjjG is a house-cleaning nucleotidase in vivo. FEMS Microbiol Lett 270:49–57. https://doi.org/10.1111/j.1574-6968.2007.00646.x.

44. Caparrós-Martín JA, McCarthy-Suárez I, Culiáñez-Macià FA. 2013. HAD hydrolase function unveiled by substrate screening: enzymatic characterization of *Arabidopsis thaliana* subclass I phosphosugar phosphatase AtSgpp. Planta 237:943–954. https://doi.org/10.1007/s00425-012-1809-5.

45. Ghorbal M, Scheidig-Benatar C, Bouizem S, Thomas C, Paisley G, Faltermeier C, Liu M, Scherf A, Lopez-Rubio J-J, Gopaul DN. 2012. Initial characterization of the Pf-Int recombinase from the malaria parasite *Plasmodium falciparum*. PLoS One 7:e46507. https://doi.org/10.1371/journal.pone.0046507.

46. Balu B, Shoue DA, Fraser MJ, Adams JH. 2005. High-efficiency transformation of *Plasmodium falciparum* by the lepidopteran transposable element piggyBac. Proc Natl Acad Sci U S A 102:16391–16396. https://doi.org/10.1073/pnas.0504679102.

47. Muralidharan V, Oksman A, Pal P, Lindquist S, Goldberg DE. 2012. *Plasmodium falciparum* heat shock protein 110 stabilizes the asparagine repeat-rich parasite proteome during malarial fevers. Nat Commun 3:1310. https://doi.org/10.1038/ncomms2306.

48. Foth BJ, Ralph SA, Tonkin CJ, Struck NS, Fraunholz M, Roos DS, Cowman AF, McFadden GI. 2003. Dissecting apicoplast targeting in the malaria parasite *Plasmodium falciparum*. Science 299:705–708. https://doi.org/10.1126/science.1078599.

49. Petersen TN, Brunak S, von Heijne G, Nielsen H. 2011. SignalP 4.0: discriminating signal peptides from transmembrane regions. Nat Methods 8:785–786. https://doi.org/10.1038/nmeth.1701.

50. Zuegge J, Ralph S, Schmuker M, McFadden GI, Schneider G. 2001. Deciphering apicoplast targeting signals–feature extraction from nuclear-encoded precursors of *Plasmodium falciparum* apicoplast proteins. Gene 280:19–26. https://doi.org/10.1016/S0378-1119(01)00776-4.

51. Mony BM, Mehta M, Jarori GK, Sharma S. 2009. Plant-like phosphofructokinase from *Plasmodium falciparum* belongs to a novel class of ATP-dependent enzymes. Int J Parasitol 39:1441–1453. https://doi.org/10.1016/j.ijpara.2009.05.011.

52. Bär J, Golbik R, Hübner G, Kopperschläger G. 2000. Denaturation of phosphofructokinase-1 from *Saccharomyces cerevisiae* by guanidinium chloride and reconstitution of the unfolded subunits to their catalytically active form. Biochemistry 39:6960–6968. https://doi.org/10.1021/bi9928142.

53. Kemp RG, Gunasekera D. 2002. Evolution of the allosteric ligand sites of mammalian phosphofructo-1-kinase. Biochemistry 41:9426–9430. https://doi.org/10.1021/bi020110d.

54. Klinder A, Kirchberger J, Edelmann A, Kopperschläger G. 1998. Assembly of phosphofructokinase-1 from *Saccharomyces cerevisiae* in extracts of single-deletion mutants. Yeast 14:323–334. https://doi.org/10.1002/(SICI)1097-0061(19980315)14:4<323::AID-YEA223>3.0.CO;2-W.

55. Theodorou ME, Cornel FA, Duff SM, Plaxton WC. 1992. Phosphate starvation-inducible synthesis of the alpha-subunit of the pyrophosphate-dependent phosphofructokinase in black mustard suspension cells. J Biol Chem 267:21901–21905.

56. Beutler E. 1984. Red cell metabolism: a manual of biochemical methods. Grune & Stratton, Philadelphia, PA.

57. Blume M, Nitzsche R, Sternberg U, Gerlic M, Masters SL, Gupta N, McConville MJ. 2015. A *Toxoplasma gondii* gluconeogenic enzyme contributes to robust central carbon metabolism and is essential for replication and virulence. Cell Host Microbe 18:210–220. https://doi.org/10.1016/j.chom.2015.07.008.

58. Brown AJP, Brown GD, Netea MG, Gow NAR. 2014. Metabolism impacts upon *Candida* immunogenicity and pathogenicity at multiple levels. Trends Microbiol 22:614–622. https://doi.org/10.1016/j.tim.2014.07.001.

59. Jurica MS, Mesecar A, Heath PJ, Shi W, Nowak T, Stoddard BL. 1998. The allosteric regulation of pyruvate kinase by fructose-1,6-bisphosphate. Structure 6:195–210. https://doi.org/10.1016/S0969-2126(98)00021-5.

60. Kronstad J, Saikia S, Nielson ED, Kretschmer M, Jung W, Hu G, Geddes JMH, Griffiths EJ, Choi J, Cadieux B, Caza M, Attarian R. 2012. Adaptation of *Cryptococcus neoformans* to mammalian hosts: integrated regulation of metabolism and virulence. Eukaryot Cell 11:109–118. https://doi.org/10.1128/EC.05273-11.

61. Cabello-Díaz JM, Gálvez-Valdivieso G, Caballo C, Lambert R, Quiles FA,

Pineda M, Piedras P. 2015. Identification and characterization of a gene encoding for a nucleotidase from *Phaseolus vulgaris*. J Plant Physiol 185:44–51. https://doi.org/10.1016/j.jplph.2015.07.008.

62. Caparrós-Martín JA, Reiland S, Köchert K, Cutanda MC, Culiáñez-Macià FA. 2007. *Arabidopsis thaliana* AtGppl and AtGpp2: two novel low molecular weight phosphatases involved in plant glycerol metabolism. Plant Mol Biol 63:505–517. https://doi.org/10.1007/s11103-006-9104-0.

63. Huang H, Pandya C, Liu C, Al-Obaidi NF, Wang M, Zheng L, Toews Keating S, Aono M, Love JD, Evans B, Seidel RD, Hillerich BS, Garforth SJ, Almo SC, Mariano PS, Dunaway-Mariano D, Allen KN, Farelli JD. 2015. Panoramic view of a superfamily of phosphatases through substrate profiling. Proc Natl Acad Sci U S A 112:E1974–E1983. https://doi.org/10.1073/pnas.1423570112.

64. Liu J, Zhou W, Liu G, Yang C, Sun Y, Wu W, Cao S, Wang C, Hai G, Wang Z, Bock R, Huang J, Cheng Y. 2015. The conserved endoribonuclease YbeY is required for chloroplast ribosomal RNA processing in *Arabidopsis*. Plant Physiol 168:205–221. https://doi.org/10.1104/pp.114.255000.

65. Daughtry KD, Huang H, Malashkevich V, Patskovsky Y, Liu W, Ramagopal U, Sauder JM, Burley SK, Almo SC, Dunaway-Mariano D, Allen KN. 2013. Structural basis for the divergence of substrate specificity and biological function within HAD phosphatases in lipopolysaccharide and sialic acid biosynthesis. Biochemistry 52:5372–5386. https://doi.org/10.1021/bi400659k.

66. Allen KN, Dunaway-Mariano D. 2009. Markers of fitness in a successful enzyme superfamily. Curr Opin Struct Biol 19:658–665. https://doi.org/10.1016/j.sbi.2009.09.008.

67. Solyakov L, Halbert J, Alam MM, Semblat J-P, Dorin-Semblat D, Reininger L, Bottrill AR, Mistry S, Abdi A, Fennell C, Holland Z, Demarta C, Bouza Y, Sicard A, Nivez M-P, Eschenlauer S, Lama T, Thomas DC, Sharma P, Agarwal S, Kern S, Pradel G, Graciotti M, Tobin AB, Doerig C. 2011. Global kinomic and phospho-proteomic analyses of the human malaria parasite Plasmodium falciparum. Nat Commun 2:565. https://doi.org/10.1038/ncomms1558.

68. Lasonder E, Green JL, Camarda G, Talabani H, Holder AA, Langsley G, Alano P. 2012. The Plasmodium falciparum schizont phosphoproteome reveals extensive phosphatidylinositol and cAMP-protein kinase A signaling. J Proteome Res 11:5323–5337. https://doi.org/10.1021/pr300557m.

69. Kochanowski K, Volkmer B, Gerosa L, Haverkorn van Rijsewijk BR, Schmidt A, Heinemann M. 2013. Functioning of a metabolic flux sensor in *Escherichia coli*. Proc Natl Acad Sci U S A 110:1130–1135. https://doi.org/10.1073/pnas.1202582110.

70. Bushell E, Gomes AR, Sanderson T, Anar B, Girling G, Herd C, Metcalf T, Modrzynska K, Schwach F, Martin RE, Mather MW, McFadden GI, Parts L, Rutledge GG, Vaidya AB, Wengelnik K, Rayner JC, Billker O. 2017. Functional profiling of a *Plasmodium* genome reveals an abundance of essential genes. Cell 170:260–272.e8. https://doi.org/10.1016/j.cell.2017.06.030.

71. Zhang M, Wang C, Otto TD, Oberstaller J, Liao X, Adapa SR, Udenze K, Bronner IF, Casandra D, Mayho M, Brown J, Li S, Swanson J, Rayner JC, Jiang RHY, Adams JH. 2018. Uncovering the essential genes of the human malaria parasite Plasmodium falciparum by saturation mutagenesis. Science 360:eaap7847. https://doi.org/10.1126/science.aap7847.

72. Penkler G, Du Toit F, Adams W, Rautenbach M, Palm DC, van Niekerk DD, Snoep JL. 2015. Construction and validation of a detailed kinetic model of glycolysis in Plasmodium falciparum. FEBS J 282:1481–1511. https://doi.org/10.1111/febs.13237.

73. van Niekerk DD, Penkler GP, Du Toit F, Snoep JL. 2016. Targeting glycolysis in the malaria parasite *Plasmodium falciparum*. FEBS J 283:634–646. https://doi.org/10.1111/febs.13615.

74. Gabryszewski SJ, Dhingra SK, Combrinck JM, Lewis IA, Callaghan PS, Hassett MR, Siriwardana A, Henrich PP, Lee AH, Gnädig NF, Musset L, Llinás M, Egan TJ, Roepe PD, Fidock DA. 2016. Evolution of fitness cost-neutral mutant PfCRT conferring *P. falciparum* 4-aminoquinoline drug resistance is accompanied by altered parasite metabolism and

digestive vacuole physiology. PLoS Pathog 12:e1005976. https://doi.org/10.1371/journal.ppat.1005976.

75. Hastings IM, Donnelly MJ. 2005. The impact of antimalarial drug resistance mutations on parasite fitness, and its implications for the evolution of resistance. Drug Resist Updat 8:43–50. https://doi.org/10.1016/j.drup.2005.03.003.

76. Rosenthal PJ. 2013. The interplay between drug resistance and fitness in malaria parasites. Mol Microbiol 89:1025–1038. https://doi.org/10.1111/mmi.12349.

77. Lim MY-X, LaMonte G, Lee MCS, Reimer C, Tan BH, Corey V, Tjahjadi BF, Chua A, Nachon M, Wintjens R, Gedeck P, Malleret B, Renia L, Bonamy GMC, Ho PC-L, Yeung BKS, Chow ED, Lim L, Fidock DA, Diagana TT, Winzeler EA, Bifani P. 19 September 2016. UDP-galactose and acetyl-CoA transporters as Plasmodium multidrug resistance genes. Nat Microbiol https://doi.org/10.1038/nmicrobiol.2016.166.

78. Corbett Y, Herrera L, Gonzalez J, Cubilla L, Capson TL, Coley PD, Kursar TA, Romero LI, Ortega-Barria E. 2004. A novel DNA-based microfluorimetric method to evaluate antimalarial drug activity. Am J Trop Med Hyg 70:119–124. https://doi.org/10.4269/ajtmh.2004.70.119.

79. Su XZ, Heatwole VM, Wertheimer SP, Guinet F, Herrfeldt JA, Peterson DS, Ravetch JA, Wellems TE. 1995. The large diverse gene family var encodes proteins involved in cytoadherence and antigenic variation of *Plasmodium falciparum*-infected erythrocytes. Cell 82:89–100. https://doi.org/10.1016/0092-8674(95)90055-1.

80. Kyes SA, Rowe JA, Kriek N, Newbold CI. 1999. Rifins: a second family of clonally variant proteins expressed on the surface of red cells infected with *Plasmodium falciparum*. Proc Natl Acad Sci U S A 96:9333–9338. https://doi.org/10.1073/pnas.96.16.9333.

81. Alexandrov A, Vignali M, LaCount DJ, Quartley E, de Vries C, De Rosa D, Babulski J, Mitchell SF, Schoenfeld LW, Fields S, Hol WG, Dumont ME, Phizicky EM, Grayhack EJ. 2004. A facile method for high-throughput co-expression of protein pairs. Mol Cell Proteomics 3:934–938. https://doi.org/10.1074/mcp.T400008-MCP200.

82. Zimmermann L, Stephens A, Nam S-Z, Rau D, Kübler J, Lozajic M, Gabler F, Söding J, Lupas AN, Alva V. 2018. A completely reimplemented MPI bioinformatics toolkit with a new HHpred server at its core. J Mol Biol 430:2237–2243. https://doi.org/10.1016/j.jmb.2017.12.007.

83. Söding J. 2005. Protein homology detection by HMM-HMM comparison. Bioinformatics 21:951–960. https://doi.org/10.1093/bioinformatics/bti125.

84. Hildebrand A, Remmert M, Biegert A, Söding J. 2009. Fast and accurate automatic structure prediction with HHpred. Proteins 77(Suppl 9):128–132. https://doi.org/10.1002/prot.22499.

85. Meier A, Söding J. 2015. Automatic prediction of protein 3D structures by probabilistic multi-template homology modeling. PLoS Comput Biol 11:e1004343. https://doi.org/10.1371/journal.pcbi.1004343.

86. Moore SA, Ronimus RS, Roberson RS, Morgan HW. 2002. The structure of a pyrophosphate-dependent phosphofructokinase from the Lyme disease spirochete *Borrelia burgdorferi*. Structure 10:659–671. https://doi.org/10.1016/S0969-2126(02)00760-8.

87. Shirakihara Y, Evans PR. 1988. Crystal structure of the complex of phosphofructokinase from *Escherichia coli* with its reaction products. J Mol Biol 204:973–994. https://doi.org/10.1016/0022-2836(88)90056-3.

88. Luo B, Groenke K, Takors R, Wandrey C, Oldiges M. 2007. Simultaneous determination of multiple intracellular metabolites in glycolysis, pentose phosphate pathway and tricarboxylic acid cycle by liquid chromatography-mass spectrometry. J Chromatogr 1147:153–164. https://doi.org/10.1016/j.chroma.2007.02.034.

89. Mullin KA, Lim L, Ralph SA, Spurck TP, Handman E, McFadden GI. 2006. Membrane transporters in the relict plastid of malaria parasites. Proc Natl Acad Sci U S A 103:9572–9577. https://doi.org/10.1073/pnas.0602293103.

90. Lim L, Linka M, Mullin KA, Weber APM, McFadden GI. 2010. The carbon and energy sources of the non-photosynthetic plastid in the malaria parasite. FEBS Lett 584:549–554. https://doi.org/10.1016/j.febslet.2009.11.097.